AUTOMATED RECONSTRUCTION OF 3D AS-BUILT BUILDING INFORMATION MODEL FOR BUILDING ENERGY PERFORMANCE ASSESSMENT

C. Kim, H. Son, and *C. Kim
Chung-Ang University
221 Heukseok-dong, Dongjak-gu
Seoul, Korea 156-756
*(*Corresponding author: changwan@cau.ac.kr)*

AUTOMATED RECONSTRUCTION OF 3D AS-BUILT BUILDING INFORMATION MODEL FOR BUILDING ENERGY PERFORMANCE ASSESSMENT

ABSTRACT

The integration of three-dimensional (3D) data with infrared thermography has received much attention for its potential use as input data for building energy simulations. Therefore, researchers have proposed methods to integrate 3D data with infrared thermography obtained by different sensors. These studies show the potential of the integration of 3D data and infrared thermography using various systems. However, these studies have ignored property aspects of infrared thermography, such as the low resolution of infrared thermography and external environmental influences. Thus, their proposed methods to integrate 3D data and infrared thermography are inadequate because these problems can affect the resulting building energy simulation. This research proposes a framework that integrates infrared thermography and 3D data while accounting for the resolution and shadow effect of infrared thermography. The proposed framework consists of three steps. In the resolution enhancement step, bi-cubic interpolation is proposed. In thermal data correction from the shadow effect, the shadow area is detected from the visible image, and then the shadow effect is removed from the registered infrared thermography. Finally, enhanced infrared thermography is mapped to the 3D data obtained by a laser scanner. The performance of the proposed framework was evaluated using test images obtained from a building in operation. The experimental results show that the proposed framework provides a 3D thermal model that is useful and accurate in simulating building energy. It is expected that the 3D thermal model can be used for accurate energy simulation of existing buildings. In addition, the proposed framework can be applied in defect detection for buildings. Furthermore, this novel approach enhances infrared thermography using visible images.

KEYWORDS

As-built model, Building information model, Building energy simulation, Infrared thermography, 3D data

INTRODUCTION

The integration of three-dimensional (3D) data with infrared thermography has received much attention for its potential use as input data for building energy simulations that aim to increase the energy efficiency of existing buildings. Building energy simulation programs requires information about buildings, such as their geometry, material, internal loads, and weather conditions (Azhar & Brown, 2009). This information directly affects the results of the building energy simulation, so it is important to obtain accurate data about the building. A laser scanner provides accurate 3D data about the geometry of a building (Kim et al., 2013). Thermal infrared cameras measure the surface temperature of external walls, doors, and windows and represent the results as infrared thermography. Infrared thermography can be used to measure emissivity (Avdelidis & Moropoulou, 2003) and the heat transfer coefficient (Fokaides & Kalogirou, 2011) of building materials. Therefore, the integration of 3D data with infrared thermography can generate information about existing buildings to support decisions about how to increase the buildings' energy efficiency.

Recently, researchers have proposed methods to integrate 3D data with infrared thermography obtained by different sensors in a different dimension. Alba et al., (2011) outlined a procedure to map infrared thermography to 3D data using a bi-camera system that consists of a thermal infrared camera and a digital camera. Before obtaining the infrared thermography and 3D data, the relative orientation and position of the thermal infrared and digital cameras are calculated based on the fixed positions of the

cameras. Then, infrared thermography and visible images are obtained using the bi-camera system, and 3D data is obtained using a laser scanner. To match the infrared thermography and 3D data, control points between the visible image and 3D data are selected manually. Wang et al., (2012) developed a hybrid system that uses a thermal infrared camera and laser scanner to fuse infrared thermography with 3D data. The relationship between infrared thermography and 3D data is built, and then, the window area is detected. Afterward, virtual 3D data for inside of the window is generated, and infrared thermography is fused to the window area. Laguela et al., (2013) proposed a method to generate an infrared thermography-textured as-built model that combines 3D data and infrared thermography without fixing the relative position of the sensors. The two-dimensional (2D) features are extracted from the infrared thermography, and the 3D features are extracted from the 3D data. Then, the infrared thermography and 3D data are registered based on the extracted 2D and 3D features. Finally, through orthographic projection, the infrared thermography-textured as-built model is generated.

These preliminary studies propose and show the potential of frameworks to integrate 3D data and infrared thermography using various systems. However, these earlier studies ignored the property aspects of infrared thermography that can affect the resulting building energy simulation. Low resolution is the first property aspect of infrared thermography. The latest thermal infrared camera obtains thermography with a resolution of only 640×480 (FLIR, 2013), which is much lower than the 3D data that obtained by a laser scanner. To accurately analyze the energy performance of existing buildings, all points in the 3D data should correspond with each pixel in the infrared thermography. However, the low resolution of infrared thermography makes it impossible to map infrared thermography to 3D data pixel-to-pixel. The second property aspect of infrared thermography is external environmental influences. The temperature value for infrared thermography may be inaccurate because of external environmental factors, such weather, sunshine, and shadows from eaves or adjacent buildings (Balaras & Argiriou 2002). Especially when obtaining infrared thermography from a building during the daytime, shadows will almost certainly be projected onto the building's exterior. These shadows will result in surface temperature measurements lower than the real temperature. Earlier studies did not consider procedures to solve these two problems, so their proposed methods to integrate 3D data and infrared thermography are unsatisfactory.

The main objective of this research is to propose a framework that integrates infrared thermography and 3D data that accounts for the resolution and shadow effect of infrared thermography. The following chapter describes the proposed framework and methods. Next, the field experimental results obtained by the proposed framework are presented, and finally, conclusions and recommendations for the direction of future research are provided.

METHODS

This research proposes a framework for integrating the 3D data and the infrared thermography to generate the 3D thermal model, and the proposed framework is shown in Figure 1. The proposed framework consists of three steps: (1) resolution enhancement of the infrared thermography; (2) thermal data correction from the shadow effect; and (3) thermal data mapping. The first step, resolution enhancement of the infrared thermography, allows for an increase of infrared thermography resolution as high as the resolution of the 3D data obtained using laser scanners. Generally, the resolution of the visible image that comes from a digital camera is higher than the resolution of the 3D data that comes from the laser scanner. Therefore, the resolution of the infrared thermography is increased as high as the resolution of the visible image. The second step is the thermal data correction from the shadow effect. The projected shadow on the external wall or window of the building results in the surface temperature being measured as lower than the real temperature. Measurement of the lower temperature because of this shadow leads to an inaccurate analysis of the building status because defect detection using infrared thermography is performed by identifying abnormal temperature areas compared with their surroundings. Therefore, the shadow effect of the infrared thermography should be removed. However, the infrared thermography contains information about the temperature, and it is difficult to detect shadows using only infrared thermography. Thus, visible images that able to detect shadows are registered with the infrared thermography, and then, the shadow area in the infrared thermography is corrected based on the detected shadow area of the registered visible image. Finally, the third step is thermal data mapping, used to map

the enhanced infrared thermography to the 3D data. By mapping the enhanced infrared thermography to the 3D data, a 3D thermal model that can be used for various applications is provided.

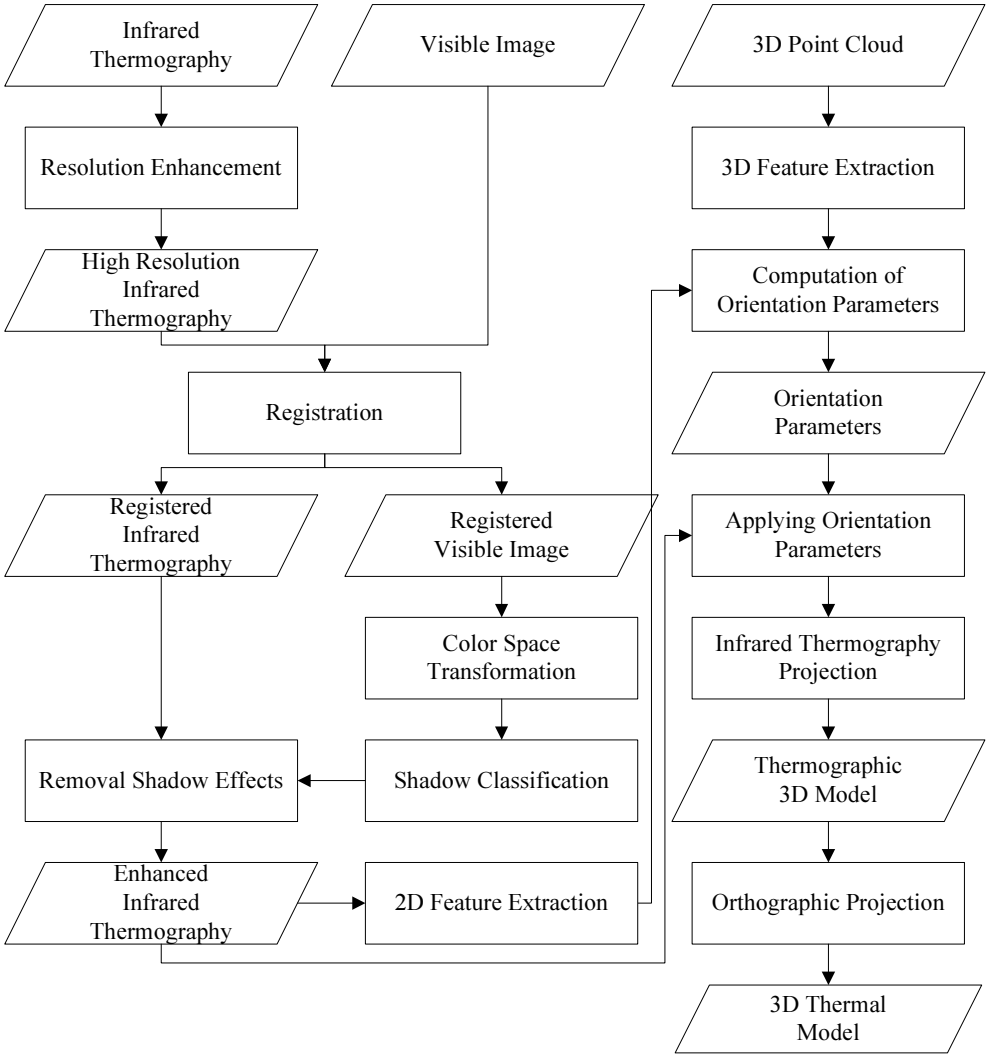

Figure 1 – Flowchart of the proposed method

Resolution Enhancement of the Infrared Thermography

Image resolution enhancement is an image processing procedure that produces a high-resolution image from a low-resolution image. The image resolution enhancement is performed by interpolation that constructs a continuous function from discrete samples (Cha & Kim, 2006). The thermal value in the infrared thermography is increased or decreased smoothly without much variation in the neighborhood at the same component or material. To account for the property of the infrared thermography, the algorithm interpolates a thermal value based on its neighborhood. The popular interpolation algorithms are nearest-neighbor, bi-linear, and bi-cubic. The bi-cubic interpolation algorithm makes smoother images than do the others (Kalpoma et al., 2013). Therefore, the bi-cubic interpolation is adapted to increase the resolution of the infrared thermography.

The bi-cubic interpolation uses 16 pixels in the nearest 4×4 neighbor in the original image to generate a new pixel. Because these 16 pixels are various distances from the new pixel, the weight is inversely proportional to the distance.

Thermal Data Correction from the Shadow Effect

The primary properties of a shadow are lower intensity, higher saturation, and higher hue values than its surroundings in the visible image (Lorenzi et al., 2012). Most shadow detection algorithms are based on these shadow properties. Early research on shadow detection noted that shadow areas have less intensity (Polidorio et al., 2003). Gray images yielded satisfactory results, but for color images, non-shadow areas with darker colors were misclassified as shadow areas. A method using chromatic information (hue and saturation) that Sarabandi et al., (2004) proposed was used to detect shadows and to remove shadow effect in a visible image. As a pre-processing step, a visible and high-resolution infrared thermography is registered before shadow detection. Then, color space transformation and shadow classification are performed on the visible image. Based on the classified shadow region in the visible image, a shadow region in the registered infrared thermography is classified. Finally, the shadow effect is removed from the infrared thermography.

Color Space Transformation

In order to classify shadow in the visible image, the color space transformation is performed. Many traditional color spaces can be used to classify shadow regions in the visible image, such as normalized rgb, Hue-Saturation-Value (HSV), $l_1l_2l_3$, and $c_1c_2c_3$ (Salvador et al., 2001). Among these color spaces, $c_1c_2c_3$ (Gevers & Smeulders, 1999) shows best results to classify shadow regions in a visible image (Salvador et al., 2001; Sarabandi et al., 2004). The $c_1c_2c_3$ color space is defined as follows:

$$c_1 = \arctan\left(\frac{R}{max(G,B)}\right) \tag{1}$$

$$c_2 = \arctan\left(\frac{G}{max(R,B)}\right) \tag{2}$$

$$c_3 = \arctan\left(\frac{B}{max(R,G)}\right) \tag{3}$$

where R, G, and B is red, green, and blue values of each pixel in the visible image.

Shadow Classification

A shadow region in the $c_1c_2c_3$ color space is an area inside of the boundary that has a pixel value different from its surroundings. Therefore, the shadow boundary is identified to classify a shadow pixel in the visible image. To identify the shadow boundary, the local variance of each pixel and its neighborhood is measured using c_3 component among c_1, c_2, and c_3 and applying a 3-by-3 filter. The local variance is defined as follows (Sarabandi et al., 2004):

$$\text{var} = \frac{1}{N}\sum_{i=0}^{N-1}\sum_{j=0}^{N-1}\left[f(i,j) - \overline{f(i,j)}\right]^2 \tag{4}$$

$$\overline{f(i,j)} = \frac{1}{N}\sum_{i=0}^{N-1}\sum_{j=0}^{N-1} f(i,j) \tag{5}$$

The high variance value is the boundary between the shadow and non-shadow region. After identifying this boundary, the shadow region is detected by classifying pixels inside of the boundary as shadows. Shadow classification in the visible image is shown in Figure 2. In Figure 2(c), the white area depicts the shadow; the black depicts the non-shadow area.

(a) (b) (c)

Figure 2 – (a) Visible image; (b) shadow boundaries from the visible image; (c) shadow detection from the visible image

Removal Shadow Effects

By detecting the shadow region in the visible image, the shadow and non-shadow regions are classified in the infrared thermography, which is registered with the visible image. The shadow effect can be removed by defining the relationship between the pixel value of the shadow region and the non-shadow region. In previous research that proposed an algorithm to remove the shadow effect in a visible image, the relationship between the pixel value of shadow and non-shadow regions was verified as reasonably linear (Lorenzi et al., 2012; Sarabandi et al., 2004). The shadow effect thus can be removed via a linear function, as shown in equation 6 (Sarabandi et al., 2004).

$$DN_{recovered} = \frac{\sigma_{non-shadow}}{\sigma_{shadow}} \left(DN_{shadow} - \mu_{shadow} \right) + \mu_{non-shadow} \tag{6}$$

where μ is the mean, and σ is the standard deviation of the shadow and non-shadow region.

Thermal Data Mapping

Thermal data mapping is performed using an automated method proposed by Laguela et al., (2013). This method has an advantage over the others in that no fixed relative position exists between sensors. Therefore, infrared thermography can be obtained from any desired position. The mapping method that Laguela et al., (2013) proposed consists of five steps. First, 2D features are extracted from the infrared thermography. Second, 3D features are extracted from the 3D data. Third, the orientation parameter is computed based on the 2D and 3D features to register thermography and 3D data. Fourth, infrared thermography projection is performed to map infrared thermography to the mesh model, which is generated from the 3D data. Finally, orthographic projection is performed to generate orthothermograms.

FIELD EXPERIMENT

Resolution Enhancement

In order to verify the performance of the bi-cubic interpolation in resolution enhancement of the infrared thermography, nearest-neighbor, bi-linear, and bi-cubic interpolation are compared. First, a test image is downsampled from 640×320 to 320×240. Then, resolution of the downsampled infrared thermography is enhanced by using nearest-neighbor, bi-linear, and bi-cubic interpolation. The resolution enhancement results of each interpolation algorithm are shown in Figure 3. In Figure 3 (a), (b), and (c) illustrate the results of nearest-neighbor, bi-linear, and bi-cubic interpolation, respectively. Figures (d), (e), and (f) are the magnified portions of Figures (a), (b), and (c), respectively. As shown in Figure 3, (d), the mosaic effect appeared in the case of nearest-neighbor interpolation. Otherwise, there is no mosaic effect in the results of bi-cubic interpolation.

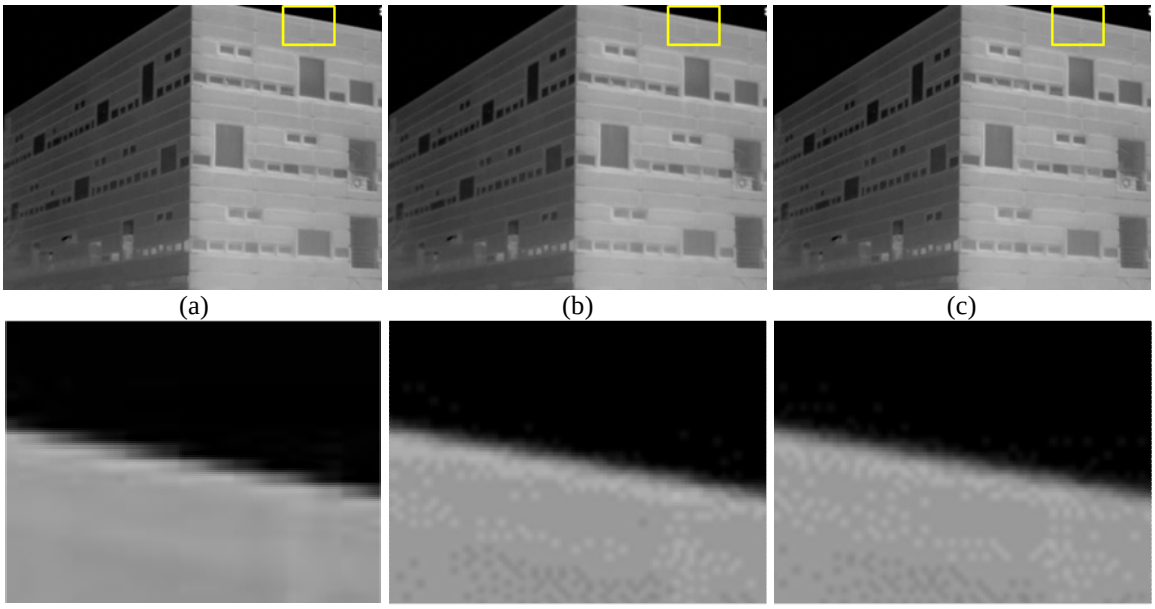

(a) (b) (c)

(d) (e) (f)

Figure 3 – (a) Nearest-neighbour interpolation; (b) bi-linear interpolation; (c) bi-cubic interpolation; (d) the magnified portion of (a); (e) the magnified portion of (b); (f) the magnified portion of (c)

To compare the nearest-neighbor, bi-linear, and bi-cubic interpolation quantitatively, Peak Signal-to-Noise Ratio (PSNR) is used. PSNR is a common measurement method in imaging processing that is used to measure the difference between two images (Aboshosha et al., 2009). A higher PSNR value means better image quality. Table 1 shows the PSNR of nearest-neighbor, bi-linear, and bi-cubic interpolation. Bi-cubic interpolation achieves the highest PSNR with test image.

Table 1 – Comparison of interpolation performance

Method	Nearest-neighbor	Bi-linear	Bi-cubic
PSNR (dB)	80.3295	83.8246	87.3500

Thermal Data Correction from the Shadow Effect

Following the procedures in the proposed method, Figure 4 shows the results of thermal data correction. As shown in Figure 4 (a), a shadow was projected onto the left external surface and holes on the right external surface of the building. The temperature value of the shadow region was lower than the real temperature in the Figure 4 (b). The dark color represents low temperature. By comparing that with the original infrared thermography, the temperature value in the shadow region was corrected in Figure 4 (c).

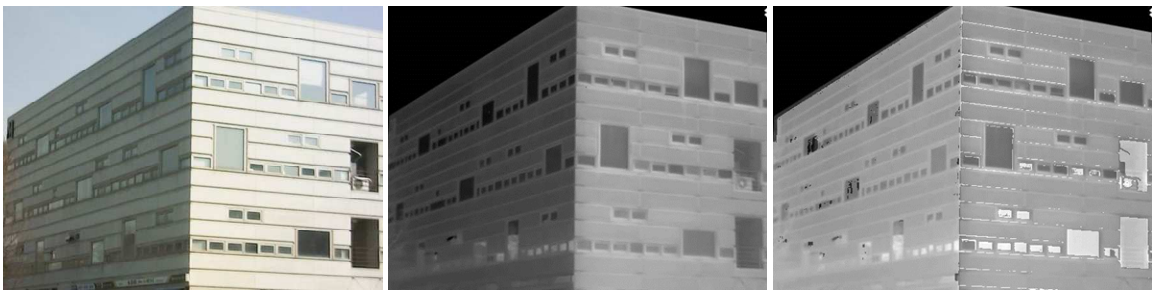

(a) (b) (c)

Figure 4 – (a) Visible image; (b) infrared thermography; (c) shadow-corrected infrared thermography

Thermal Data Mapping

Following resolution enhancement and thermal data correction from the shadow effect, infrared thermography is high-resolution and contains corrected thermal data from the shadow effect. This thermography is applied to the 3D data by using a 2D/3D matching method, such as the one described that Laguela et al., (2013) described. Figure 5 shows the 3D thermal model generated by using this 2D/3D matching method. This 3D thermal model contains accurate information that can be used to simulate building energy.

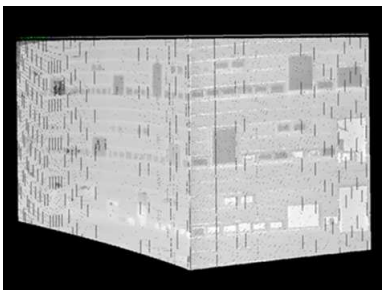

Figure 5 – 3D Thermal model

CONCLUSIONS

This research proposed a framework that integrates infrared thermography and 3D data in consideration of the resolution and shadow effect of the infrared thermography. In order to integrate the infrared thermography and the 3D data, the framework involved three steps: (1) resolution enhancement of the infrared thermography; (2) thermal data correction from the shadow effect; and (3) thermal data mapping. The experimental results show that the proposed framework provides a 3D thermal model that is applicable to simulate building energy. It is expected that the 3D thermal model can be used for accurate energy simulation of the existing building. In addition, the proposed framework can be applied to defect detection for the building. Furthermore, this novel approach was proposed to enhance infrared thermography using visible images. This fusion approach of these different kinds of sensors will be the best way to enhance the data.

Although interesting results have been achieved, still further methodological improvements are required. First, bi-cubic interpolation generates blur effects and loses edge-information of the object. In order to overcome the shortcoming of the bi-cubic interpolation, the adaptive interpolation algorithm that applies different interpolation algorithms according to direction of the edge will be proposed. Second, a problem still exists with the detection of dark objects as shadows. To accurately detect shadow regions, other features will be used to classify shadows in the visible image. In addition, future research will focus on the generation of a physical model to use as input for the building energy simulation program.

ACKNOWLEDGMENTS

This research was supported by a grant (12 Hightech Urban C02) from High-tech Urban Development Program funded by Ministry of Land, Transport and Maritime Affairs of Korean government.

REFERENCES

Aboshosha, A., Hassan, M., Ashour, M., & El Mashade, M. (2009, December). Image denoising based on spatial filters, an analytical study. Paper session presented at the International Conference on Computer Engineering & Systems, Cairo, Egypt.

Alba, M. I., Barazzetti, L., Marco, S., Rosina, E., & Previtali, M. (2011). Mapping infrared data on terrestrial laser scanning 3D models of buildings. *Remote Sensing*, 3, 1847-1870. doi: 10.3390/rs3091847

Avdelidis, N. P., & Moropoulou, A. (2003). Emissivity considerations in building thermography. *Energy and Buildings*, 35, 663-667. doi: 10.1016/S03787788

Azhar, S., & Brown, J. (2009). BIM for sustainability analyses. *International Journal of Construction Education and Research*, 5, 276-292. doi: 10.1080/15578770903355657

Balaras, C. A., & Argiriou, A. A. (2002). Infrared thermography for building diagnostics. *Energy and Buildings*, 34, 171-183. doi: 10.1016/S03787788

Cha, Y., & Kim, S. (2006). Edge-forming methods for image zooming. *Journal of Mathematical Imaging and Vision*, 25, 353-364. doi: 0.1007/s1085100672502

FLIR (2013). Specifications of FLIR T620 & T640. Retrieved from http://www.flir.com

Fokaides, P. A., & Kalogirou, S. A. (2011). Application of infrared thermography for the determination of the overall heat transfer coefficient (U-value) in building envelopes. *Applied Energy*, 88, 4358-4365. doi: 10.1016/j.apenergy.2011.05.014

Gevers, T., & Smeulders, A. W. M. (1999). Color-based object recognition. *Pattern Recognition*, 32, 453-464. doi: 10.1016/S0031-3203(98)00036-3

Kalpoma, K. A., Kawano, K., & Kudoh, J. (2013). IKONOS image fusion process using steepest descent method with bi-linear interpolation. *International Journal of Remote Sensing*, 34, 505-518. doi: 10.1080/01431161.2012.712233

Kim, C., Son, H., & Kim. C. (2013). Automated construction progress measurement using a 4D building information model and 3D data. *Automation in Construction*, 31, 75-82. doi: 10.1016/j.autcon.2012.11.041

Laguela, S., Diaz-Vilarino, L., & Armesto, M. J. (2013). Automatic thermographic and RGB texture of as-built BIM for energy rehabilitation purposes. *Automation in Construction*, 31, 230-240. doi: 10.1016/j.autcon.2012.12.013

Lorenzi, L., Melgani, F., & Mercier, G. (2012). A complete processing chain for shadow detection and reconstruction in VHR images. *IEEE Transaction on Geoscience and Remote Sensing*, 50, 3440-3452. doi: 10.1109/TGRS.2012.2183876

Polidorio, A. M., Flores, F. C., Imai, N. N., Tommaselli, A. M. G., & Franco, C. (2003, October). Automatic shadow segmentation in aerial color images. Paper session presented at the 16th Brazilian Symposium on Computer Graphics and Image Processing, Sao Carlos, Brazil.

Salvador, E., Cavallaro, A., & Ebrahimi, T. (2001, October). Shadow identification and classification using invariant color models. Paper session presented at the 2001 IEEE International Conference on Acoustics, Speech, and Signal Processing, Salt Lake City, UT.

Sarabandi, P., Yamazaki, F., Matsuoka, M., & Kiremidjian, A. (2004, September). Shadow detection and radiometric restoration in satellite high resolution images. Paper session presented at the 2004 IEEE International Geoscience and Remote Sensing Symposium, Anchorage, AK.

Wang, C., Cho, Y. K., & Gai, M. (2012). As-is 3D thermal modeling for existing building envelopes using a hybrid LIDAR system. *Journal of Computing in Civil Engineering*, in press. doi: 10.1061/(ASCE)CP.1943-5487.0000273